Crossover from ferromagnetic to antiferromagnetic ground state in the $(Ce_{1-x}U_x)_2Pd_{2.05}Sn_{0.95}$ system

1999 J. Phys.: Condens. Matter 11 5195

(http://iopscience.iop.org/0953-8984/11/26/320)

J. Phys.: Condens. Matter **11** (1999) 5195–5208. Printed in the UK PII: S0953-8984(99)01682-3

Crossover from ferromagnetic to antiferromagnetic ground state in the $(Ce_{1-x}U_x)_2Pd_{2.05}Sn_{0.95}$ system

D Laffargue†‡, S Bordère†, F Bourée‡, B Chevalier†§, J Etourneau† and T Roisnel‡

† Institut de Chimie de la Matière Condensée de Bordeaux (ICMCB), CNRS (UPR 9048), Université Bordeaux I, Avenue du Docteur A Schweitzer, 33608 Pessac Cédex, France
‡ Laboratoire Léon Brillouin (CEA-CNRS), CEA/Saclay, 91191 Gif-sur-Yvette Cédex, France

E-mail: chevalie@icmcb.u-bordeaux.fr

Received 8 February 1999, in final form 20 April 1999

Abstract. The $(Ce_{1-x}U_x)_2Pd_{2.05}Sn_{0.95}$ solid solution has been investigated by means of x-ray powder diffraction and magnetization measurements. All the compounds crystallize in the tetragonal U_2Fe_2Sn-type structure, $P4/mbm$ space group. A crossover from ferromagnetic to antiferromagnetic behaviour at low temperature is observed around $x \simeq 0.30$: in the composition range $0 \leqslant x < 0.30$, the Curie tempertaure T_C goes through a maximum at $x \simeq 0.10$–0.15 whereas for $0.30 \leqslant x < 1.0$ the Néel temperature T_N increases continuously with x. Neutron powder diffraction performed on $(Ce_{0.85}U_{0.15})_2Pd_{2.05}Sn_{0.95}$ ($x = 0.15$) confirms the existence of a ferromagnetic structure below $T_C = 4.6(1)$ K, with (Ce, U) magnetic moments parallel to the tetragonal c-axis. The magnetic phase diagram ((T_C, T_N) against x) of this system is discussed considering a Ruderman–Kittel–Kasuya–Yosida model based on a non-spherical Fermi surface.

1. Introduction

Ternary stannides $R_2Pd_{2+y}Sn_{1-y}$ with $R =$ rare earth, uranium or neptunium have recently been the subject of great interest due to the large variety of their magnetic properties [1–14]. All the compounds crystallize in the tetragonal U_2Fe_2Sn-type structure, $P4/mbm$ space group [1]. Moreover, previous works on these ternary stannides with R = Ce [4, 5], Nd [13], Gd, Tb, Dy, Ho, Er [12] and U [3] have shown the existence of a homogeneity range on the palladium rich side ($y > 0$). For instance, the solid solutions $Ce_2Pd_{2+y}Sn_{1-y}$ and $U_2Pd_{2+y}Sn_{1-y}$ respectively exist for $0.04(3) \leqslant y \leqslant 0.21(4)$ [5] and $0 \leqslant y \leqslant 0.44(2)$ [3].

The ternary stannides $Ce_2Pd_{2+y}Sn_{1-y}$ excepted, all compounds order antiferromagnetically at low temperature, with magnetic structures depending on the nature of R-element. For instance, U_2Pd_2Sn exhibits below $T_N = 40(1)$ K a non-collinear arrangement of the U-magnetic moment with $\boldsymbol{k} = (0\,0\,0)$ as propagation vector [7, 8]. Two antiferromagnetic transitions, at 27.3(2) K and 20.8(5) K, are observed for $Tb_2Pd_{2.05}Sn_{0.95}$ corresponding respectively to the occurrence of incommensurate ($\boldsymbol{k} = (k_x k_x 1/2)$) and commensurate ($\boldsymbol{k} = (0\,0\,1/2)$) non-collinear magnetic structures [11]. Among these ternaries, $Ce_2Pd_{2.05}Sn_{0.95}$ exhibits a unique magnetic behaviour: for this compound, the sequence 'paramagnetic $\rightarrow$ antiferromagnetic $\rightarrow$ ferromagnetic' is observed with decreasing T, with Néel and Curie temperatures respectively equal to $T_N = 4.8(2)$ K and $T_C = 3.0(2)$ K [11]. Similar magnetic transitions were obtained for the ternary indide Ce_2Pd_2In [15, 16].

§ Corresponding author.

0953-8984/99/265195+14$19.50

With this view, it seems interesting to study the influence of the substitution of R for Ce on the stability of the ferromagnetic phase. In this paper, we report on the structural and magnetic properties of the $(Ce_{1-x}U_x)_2Pd_{2.05}Sn_{0.95}$ solid solution: magnetization measurements give the magnetic phase diagram ((T_N, T_C) against x) of the system; and neutron powder diffraction the magnetic structure of $(Ce_{0.85}U_{0.15})_2Pd_{2.05}Sn_{0.95}$ ($x = 0.15$). Finally, the experimental magnetic phase diagram ((T_N, T_C) against x) is compared to that calculated from an anisotropic Ruderman–Kittel–Kasuya–Yosida (RKKY) model recently described by us [17].

2. Experimental details

Polycrystalline samples were prepared by melting of the constituent elements under a purified argon atmosphere in an induction levitation furnace. The obtained ingots were then annealed under vacuum at 800 °C for one month. Using x-ray powder diffraction (Guinier camera, Cu Kα radiation), all the samples were confirmed to be single phased with tetragonal U_2Fe_2Sn-type structure. The unit cell parameters a and c (table 1) are both decreasing with increasing x, owing to the smaller metallic radius of uranium (0.156 nm) as compared to cerium (0.1825 nm). The composition dependence of these parameters follows practically a simple Vegard law (figure 1). In this U_2Fe_2Sn-type structure, the Ce (or U) atoms form a three-dimensional network of [Ce, U]$_6$ and [Ce, U]$_8$ prisms respectively surrounding Pd and Sn atoms with the excess of Pd atoms (in this work 0.05 formula units). Each Ce (or U) species has seven Ce (or U) nearest neighbours: (i) five (4 + 1) are located in the (a, b)-plane with interatomic distances labelled d_4 and d_1; (ii) two are along the c-axis with d_2-spacing [5, 8]. The smallest distance corresponds to atoms respectively located in the (a, b)-plane for $Ce_2Pd_{2.05}Sn_{0.95}$ ($d_1 = 0.3910(1)$ nm) and along the c-axis for $U_2Pd_{2.05}Sn_{0.95}$ ($d_2 = 0.3782(1)$ nm). This structural change plays a role in the magnetocrystalline anisotropy observed for these compounds: the directions of the magnetic moments in $Ce_2Pd_{2.05}Sn_{0.95}$ and $U_2Pd_{2.05}Sn_{0.95}$ are perpendicular to the direction of the d_i-minimum. Let us note that for the $(Ce_{1-x}U_x)_2Pd_{2.05}Sn_{0.95}$ solid solution, d_1- and d_2-distances are nearly identical at $T = 300$ K in the composition range with $x \simeq 0.25$–0.30: respectively 0.3893(1) and 0.3899(1) nm for $x = 0.25$ and 0.3894(1) and 0.3886(1) nm for $x = 0.30$. Certainly this structural consideration could explain, around $x \simeq 0.25$–0.30, a change in the magnetic properties of the considered solid solution.

Table 1. Crystallographic and magnetic data relative to $(Ce_{1-x}U_x)_2Pd_{2.05}Sn_{0.95}$ ternary stannides (uncertainties of the least-significant digits are given in parentheses throughout the paper).

	Crystallographic data			Magnetic data				
x	a (nm)	c (nm)	V_m (nm^3)	C_m (emu mol^{-1} K^{-1})	θ_p (K)	T_N (K)	T_C (K)	Ref.
0	0.7762	0.3930	0.2368	1.72	−20	4.7(2)	3.0(2)	[5]
0.10	0.7747(1)	0.3933(1)	0.2360(1)	1.69(2)	−19(1)		5.6(2)	[a]
0.15	0.7745(1)	0.3918(1)	0.2350(1)	1.76(2)	−44(1)		5.0(2)	[a]
0.20	0.7740(1)	0.3909(1)	0.2342(1)	1.73(2)	−30(1)		3.7(2)	[a]
0.25	0.7729(1)	0.3899(1)	0.2329(1)	1.75(2)	−26(1)		2.8(2)	[a]
0.30	0.7731(1)	0.3886(1)	0.2323(1)	1.85(2)	−32(1)			[a]
0.40	0.7718(1)	0.3868(1)	0.2304(1)	1.89(2)	−36(1)	10.0(5)		[a]
0.60	0.7670(1)	0.3850(1)	0.2265(1)	2.18(2)	−60(1)	23.5(5)		[a]
0.80	0.7643(1)	0.3819(1)	0.2231(1)	2.13(2)	−70(1)	33.0(5)		[a]
1.0	0.7603	0.3785	0.2188	2.00	−50	41		[7]
1.0	0.7610	0.3782	0.2190			40(1)		[8]

[a] This work.

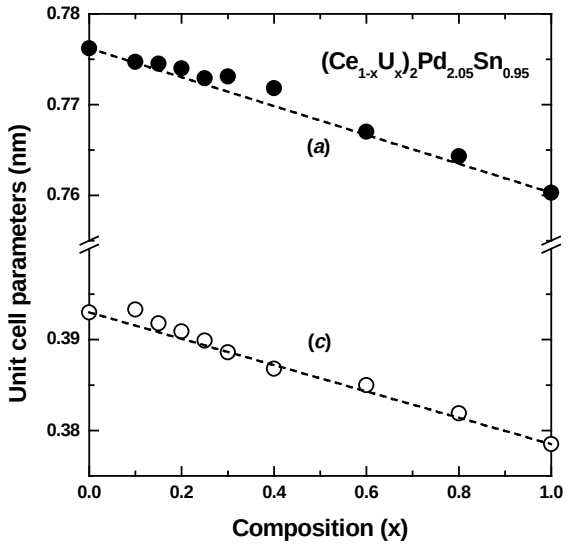

Figure 1. Composition dependence of the unit cell parameters (a (full symbols) and c (open symbols)) for $(Ce_{1-x}U_x)_2Pd_{2.05}Sn_{0.95}$ stannides (the sizes of the symbols are much bigger than the uncertainty on the data).

The magnetization was measured above 2 K on the polycrystalline samples in a conventional superconducting quantum interference device (SQUID) magnetometer.

Neutron powder diffraction experiments were performed for $(Ce_{1-x}U_x)_2Pd_{2.05}Sn_{0.95}$ ($x = 0.15$), at the Orphée reactor (CEA/Saclay, France) on the two-axis diffractometer G4.1 (800-cell position sensitive detector, $\lambda = 0.2426$ nm). The structural refinements were carried out using the Rietveld profile method, with FULLPROF program [18], scattering lengths from [19] and Ce^{3+}, U^{3+} magnetic form factors from [20, 21].

3. Results and discussion

3.1. Magnetization measurements

The thermal dependence of the reciprocal magnetic susceptibility χ_m^{-1} is shown in figure 2 for selected compositions ($x = 0.10$, 0.30 and 0.60). Above 75–100 K, all the $\chi_m^{-1} = f(T)$ curves can be fitted by a Curie–Weiss law, leading to the Curie constant (C_m) and paramagnetic Curie temperature (θ_p) summarized in table 1. At low temperatures, the deviation of $\chi_m^{-1} = f(T)$ curves from Curie–Weiss behaviour is typical of magnetic intermetallics based on Ce or U, and is generally attributed to the effect of crystal field. The C_m-value exhibits a tendency to increase with x in agreement with the effective moment $\mu_{eff} = (8(C_m/2))^{1/2}$, which is higher in U_2Pd_2Sn ($\mu_{eff} = 2.83\ \mu_B$/U) [7] than in $Ce_2Pd_{2.05}Sn_{0.95}$ ($\mu_{eff} = 2.62\ \mu_B$/Ce) [5]. Moreover, for all compositions, the θ_p-temperature is always negative.

The thermal dependence of the magnetization (Mag.) of $(Ce_{1-x}U_x)_2Pd_{2.05}Sn_{0.95}$ compounds measured in low field $B = 0.01$ T exhibits several behaviours, depending on the composition (figure 3): (i) for $0 < x \leqslant 0.25$, (Mag.) increases sharply below T_C (T_C is defined by the occurrence of a minimum in the derivative curve d(Mag.)/d$T = f(T)$) as for a ferromagnetic materials (figure 3(a)); (ii) no anomaly is detected down to 2 K in the (Mag.) $= f(T)$ curve for $x = 0.30$ (figure 3(b)); between 2 K and 8 K, the magnetic

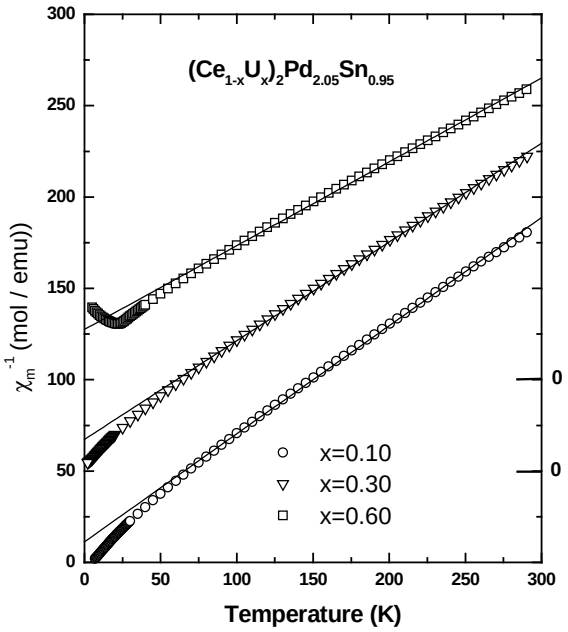

Figure 2. Temperature dependence of the reciprocal magnetic susceptibility of some $(Ce_{1-x}U_x)_2Pd_{2.05}Sn_{0.95}$ stannides ($x = 0.10$, 0.30 and 0.60). The Curie–Weiss law is indicated by a solid line. (For the sake of clarity, the curves were shifted by 50 along the χ_m^{-1} axis.)

susceptibility of this stannide follows a Curie–Weiss law with $C_m = 0.96(2)$ and $\theta_p = -3(1)$ K as parameters; (iii) in contrast, for $x \geqslant 0.40$ the magnetization goes through a maximum characteristic of the appearence of antiferromagnetic ordering below T_N (figure 3(c)). This study shows then the existence at $x \simeq 0.30$ in the $(Ce_{1-x}U_x)_2Pd_{2.05}Sn_{0.95}$ system of a crossover from ferromagnetic to antiferromagnetic state at low temperature. The magnetic ordering temperatures (T_C or T_N) are given in table 1. In contrast to what exists for $Ce_2Pd_{2.05}Sn_{0.95}$ where an antiferromagnetic $\rightarrow$ ferromagnetic transition is observed as the temperature is lowered [5, 9], no similar behaviour is detected for instance for $(Ce_{0.9}U_{0.1})_2Pd_{2.05}Sn_{0.95}$ stannide.

This magnetic 'crossover' in the $(Ce_{1-x}U_x)_2Pd_{2.05}Sn_{0.95}$ system is confirmed by magnetization (Mag.) measurements at $T = 2$ K in applied magnetic fields B up to 5 T (figure 4): (i) for $x = 0.10$ and 0.15, (Mag.) increases strongly at low fields, then almost saturates (figure 4(a)); such a behaviour is typical of ferromagnetism and we note for this composition range ($0 \leqslant x \leqslant 0.15$) an increase of (Mag.) at $B = 4.5$ T with increasing x, indicating that the ferromagnetic interaction is stronger and stronger (let us recall that (Mag.) $=1.64(2)\ \mu_B\ \text{mol}^{-1}$ at $T = 2$ K and $B = 4.5$ T for $Ce_2Pd_{2.05}Sn_{0.95}$ [5]; (ii) no saturation is observed in the (Mag.) $= f(B)$ curves for $x = 0.25$ and 0.30 (figure 4(a)) supporting the fact that ferromagnetic interactions weaken then as uranium composition increases; (iii) for $x > 0.30$ (figure 4(b)) (Mag.) becomes small and varies almost linearly with B, except for $x = 0.40$, where the curve (Mag.) $= f(B)$ increases more rapidly above a critical field $B \simeq 3$ T suggesting there the occurrence of a metamagnetic transition.

The magnetic phase diagram of the $(Ce_{1-x}U_x)_2Pd_{2.05}Sn_{0.95}$ system deduced from our magnetization measurements is presented on figure 5. We can distinguish three distinct

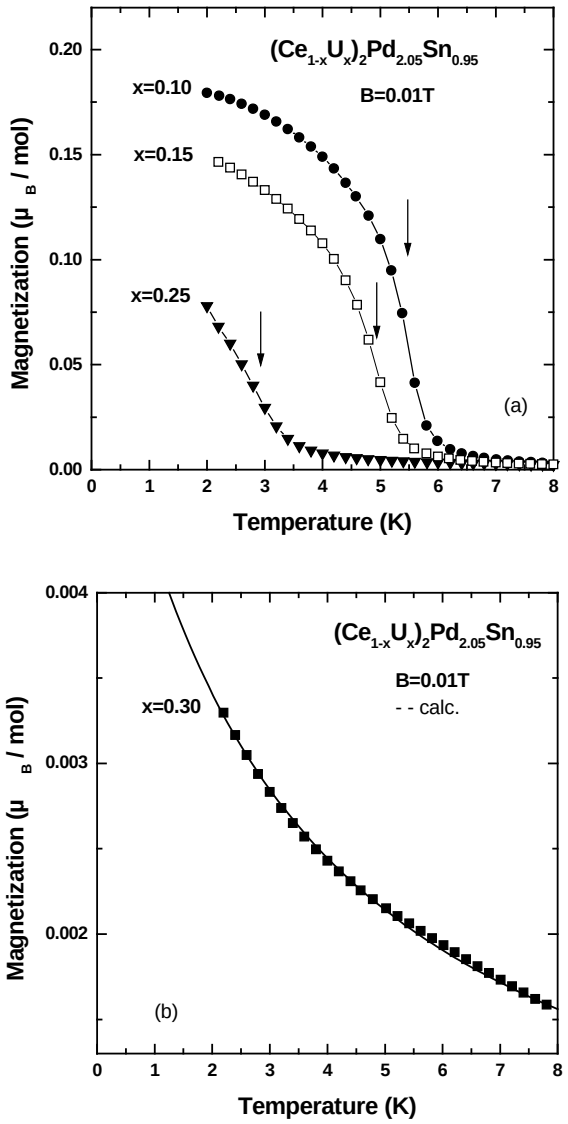

Figure 3. Temperature dependence of the magnetization of $(Ce_{1-x}U_x)_2Pd_{2.05}Sn_{0.95}$ stannides measured in an applied field $B = 0.01$ T: (a) for $0 < x \leqslant 0.25$; (b) for $x = 0.30$ (the solid line is a Curie–Weiss fit ($T \leqslant 8$ K)) and (c) for $0.40 \leqslant x < 1.0$. The arrows indicate the Curie or Néel temperature.

magnetic phases: (i) for $0 \leqslant x < 0.30$ a ferromagnetic arrangement is stable below T_C (Curie temperature) with T_C going through a maximun around $x \simeq 0.10$–0.15; (ii) for $0.30 < x \leqslant 1.0$ an antiferromagnetic phase exists below T_N (Néel temperature) and T_N increases continuously with x; (iii) no magnetic transition appears down to 2 K for $x = 0.30$. This x-value corresponds to the boundary between ferromagnetic and antiferromagnetic behaviours; for this stannide, the competition between ferromagnetic and antiferromagnetic interactions is responsible for magnetic 'frustration'.

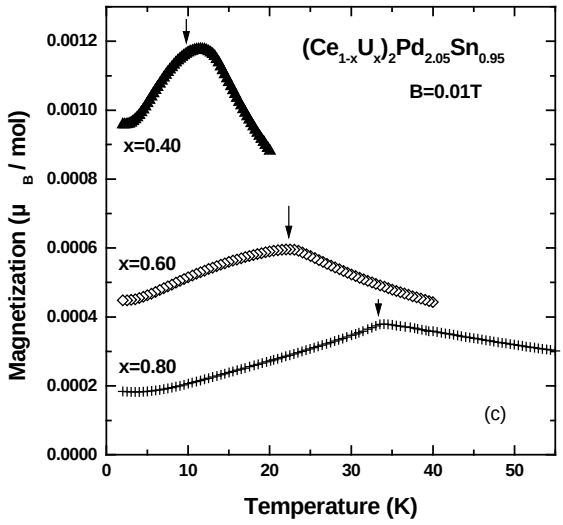

Figure 3. (Continued)

3.2. Magnetic structure of $(Ce_{0.85}U_{0.15})_2Pd_{2.05}Sn_{0.95}$

Among ferromagnetic $(Ce_{1-x}U_x)_2Pd_{2.05}Sn_{0.95}$ stannides, $(Ce_{0.85}U_{0.15})_2Pd_{2.05}Sn_{0.95}$ exhibits the highest T_C-temperature obtained for the ferromagnetic phase (figure 5). In order to verify that this stannide presents only one magnetic transition (paramagnetic $\rightarrow$ ferromagnetic) in contrast to the $Ce_2Pd_{2+y}Sn_{1-y}$ system which shows a paramagnetic $\rightarrow$ antiferromagnetic $\rightarrow$ ferromagnetic sequence [9, 22], we have performed its investigation by neutron powder diffraction.

Neutron powder diffraction patterns of $(Ce_{0.85}U_{0.15})_2Pd_{2.05}Sn_{0.95}$ at low temperature (1.5 K $\leqslant T \leqslant$ 8.4 K) are shown in figure 6. At 8.4 K in the paramagnetic domain, the pattern exhibits only nuclear Bragg peaks (for instance (1 1 0) and (0 0 1)), in agreement with the crystal structure ($P4/mbm$ space group, U_2Fe_2Sn-type structure). Below 5 K in the ordered magnetic domain, the patterns do not show any additional reflections (with respect to the nuclear spectrum) but an intensity increase of the (1 1 0), (2 0 0) and (2 1 0) Bragg peaks, which can be accounted for by the occurrence of ferromagnetic ordering. The absence of any magnetic contribution to (0 0 1) reflection clearly indicates that the magnetic moments (Ce and U cannot be distinguished by their magnetic form factors in the considered angular range) are parallel to the tetragonal c-axis. Table 2 compares experimental and calculated magnetic intensities at $T = 1.5$ K for the best agreement factor ($R_M = 8.2\%$); the value of the (Ce, U) magnetic moment is then 1.20(3) μ_B. The same magnetic arrangement was described for ferromagnetic $Ce_2Pd_{2.04}Sn_{0.96}$ below 3.0 K [5, 9].

Moreover, the thermal dependence of $(Ce_{0.85}U_{0.15})_2Pd_{2.05}Sn_{0.95}$ neutron powder diffraction patterns shows that this stannide exhibits only one magnetic transition, from paramagnetism to ferromagnetism, in contrast to the case of the $Ce_2Pd_{2+y}Sn_{1-y}$ system. From the thermal dependence of (2 0 0) and (2 1 0) magnetic intensities (figure 7), one obtains $T_C = 4.6(1)$ K as the Curie temperature, in good agreement with $T_C = 5.0(2)$ K, as deduced from magnetization measurements (table 1). Moreover, the absence of visible saturation on these last curves (clearly observable for the (2 1 0) reflection) shows that the magnetic moment calculated at 1.5 K is underestimated.

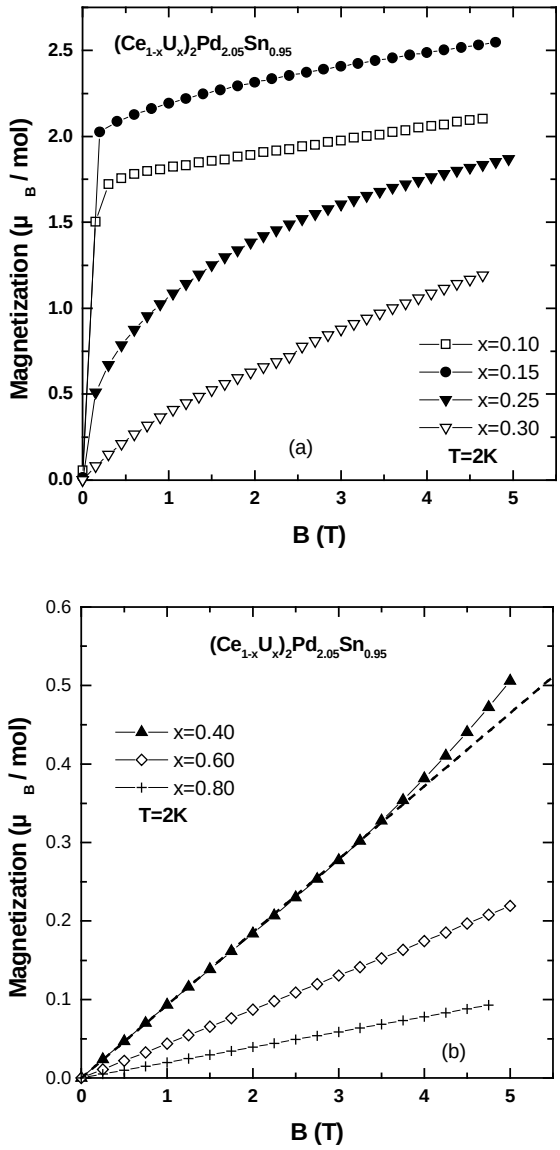

Figure 4. Field dependence at $T = 2$ K of the magnetization of some $(Ce_{1-x}U_x)_2Pd_{2.05}Sn_{0.95}$ stannides: (a) for $0 < x \leqslant 0.30$ and (b) for $0.40 \leqslant x < 1.0$.

3.3. Calculated magnetic phase diagram of the $(Ce_{0.85}U_{0.15})_2Pd_{2.05}Sn_{0.95}$ system

Recently, we reproduced the composition dependence of the Néel temperature in the $U_2(Ni_{1-x}Pd_x)_2Sn$ system ($T_N = f(x)$ curve) using a Ruderman–Kittel–Kasuya–Yosida (RKKY) model based on a non-spherical Fermi surface [17]. The minimum of T_N against x observed in this system near $x \simeq 0.30$–0.35 was then explained by the occurrence of a transition between two antiferromagnetic structures: collinear $\boldsymbol{k} = (0\,0\,1/2)$ as for U_2Ni_2Sn [23] and non-collinear $\boldsymbol{k} = (0\,0\,0)$ as for U_2Pd_2Sn [7, 8]. Neutron powder diffraction performed on the two stannides $U_2(Ni_{0.70}Pd_{0.30})_2Sn$ and $U_2(Ni_{0.55}Pd_{0.45})_2Sn$ [24, 25] confirmed this magnetic

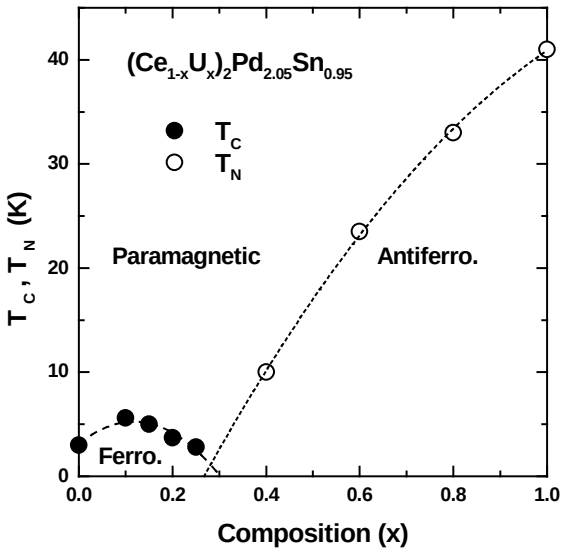

Figure 5. $((T_C, T_N)$–$x)$ magnetic phase diagram of the $(Ce_{1-x}U_x)_2Pd_{2.05}Sn_{0.95}$ system, as deduced from magnetization measurements.

Table 2. Comparison of calculated and experimental neutron powder diffraction magnetic intensities ($T = 1.5$ K) for ferromagnetic stannide $(Ce_{0.85}U_{0.15})_2Pd_{2.05}Sn_{0.95}$.

hkl	2θ (°)	$I_{calc.}$ (barn mol^{-1})	$I_{exp.}$ (barn mol^{-1})
1 0 0	18.7(1)	0	0
1 1 0	26.3(1)	15.8	14.5(5)
0 0 1	36.5(1)	0	0
2 0 0	37.2(1)	61.6	70.8(5)
1 0 1	41.1(1)	0	0
2 1 0	41.7(1)	195.2	178.3(5)

transition suggesting accordingly the validity of the anisotropic RKKY model. It is then interesting to investigate whether such a model could account for the magnetic properties of the $(Ce_{1-x}U_x)_2Pd_{2.05}Sn_{0.95}$ system. We note that this system is complex on account of the occurrence versus composition of the ferromagnetic $\rightarrow$ antiferromagnetic transition ($x \simeq 0.30$) which induces magnetic frustration at the borderline. This leads to the existence of disorder near the critical composition.

Considering the interaction constant j_{sf} between the spins of localized f and conduction electrons as constant, the indirect exchange RKKY mechanism [26–28] leads to a simple expression of the exchange integral J_{ij} between the spins, S_i and S_j of the two atoms i and j, respectively located at R_i and R_j (J_{ij} depends both on the Fermi wavevector k_F and on the interatomic distances R_{ij}) [26]. The extension of this expression when considering anisotropic instead of isotropic free electron effective mass leads to the subsequent exchange integral [17]:

$$J_{ij} = J(k_F, R'_{ij}) = \frac{9\pi}{4}\frac{n_0^2}{E_F} j_{sf}^2 \left(\frac{\sin(2k_F R'_{ij}) - (2k_F R'_{ij})\cos(2k_F R'_{ij})}{(2k_F R'_{ij})^4} \right). \quad (1)$$

The only change in the formula lies in R'_{ij} (instead of R_{ij}), which are now 'adjusted' distances between i and j atoms and depend on the mass anisotropy. For the tetragonal

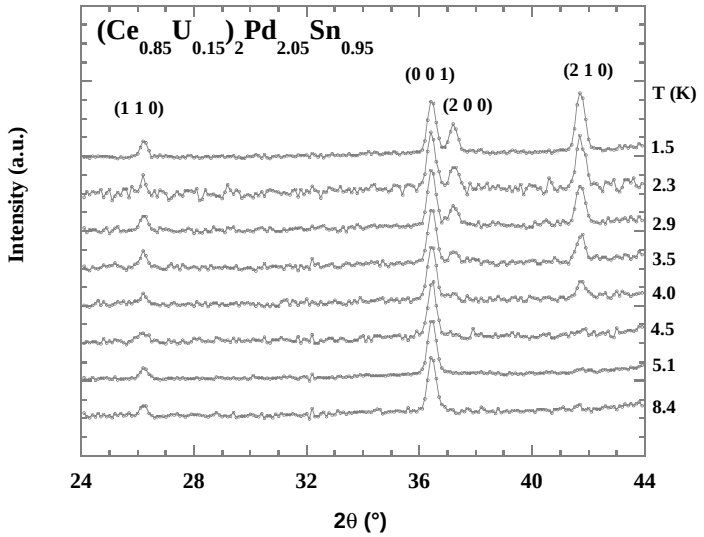

Figure 6. Neutron powder diffraction patterns ($1.5\,\mathrm{K} \leqslant T \leqslant 8.4\,\mathrm{K}$) for $(Ce_{0.85}U_{0.15})_2Pd_{2.05}Sn_{0.95}$ stannide.

$(Ce_{1-x}U_x)_2Pd_{2.05}Sn_{0.95}$ system, uniaxial anisotropy is considered with $m_x = m_y = m \neq m_z$ (z along the tetragonal c-axis). The R'_{ij} values are thus expressed as:

$$R'_{ij} = \sqrt{R^2_{ijx} + R^2_{ijy} + \frac{m_z}{m} R^2_{ijz}}$$

where R_{ijx}, R_{ijy}, R_{ijz} are the projections of the R_{ij} interatomic distance on the a-, b- and c-axes, respectively; k_F is the Fermi wavevector component in the ab-plane; E_F is the Fermi energy and n_0 the number of conduction electrons per unit cell of the crystal structure. E_F and n_0 are linked to the Fermi wavevector components, k_F (lying in the ab-plane) and k_{Fz} (parallel to the c-axis) via (V_0 = unit cell volume)

$$E_F = \frac{\eta^2 k_F^2}{2m} = \frac{\eta^2 k_{Fz}^2}{2m_z} \qquad n_0 = \frac{k_F^2 k_{Fz}}{3\pi^2} V_0.$$

The Heisenberg magnetic energy of the $(Ce_{1-x}U_x)_2Pd_{2.05}Sn_{0.95}$ system is then given as

$$E = -\frac{N}{n_c} \sum_{i=1}^{n_c} \sum_{\substack{j \neq i \\ j=1}}^{N} J(k_F, R'_{ij}) S_i \cdot S_j \tag{2}$$

n_c being the number of (Ce, U) atoms in the magnetic unit cell. Using the mean-field approximation, the order–disorder magnetic transition temperature is consequently [29] given by the formula

$$T_C \text{ or } T_N = \frac{(g_J - 1)^2 J(J+1)}{3k_B} \frac{1}{n_c} \sum_{i=1}^{n_c} \sum_{\substack{j \neq i \\ j=1}}^{N} J(k_F, R'_{ij}) \frac{M_i \cdot M_j}{M^2} \tag{3}$$

where $(g_J - 1)^2 J(J+1) = G$ is the De Gennes factor with g_J = Landé factor and J = total angular momentum of the magnetic ion; M_i, M_j are the magnetic moments located at R_i, R_j, with the assumption $\|M_i\| = \|M_j\| = M$, M being the value of the (Ce, U) magnetic moment.

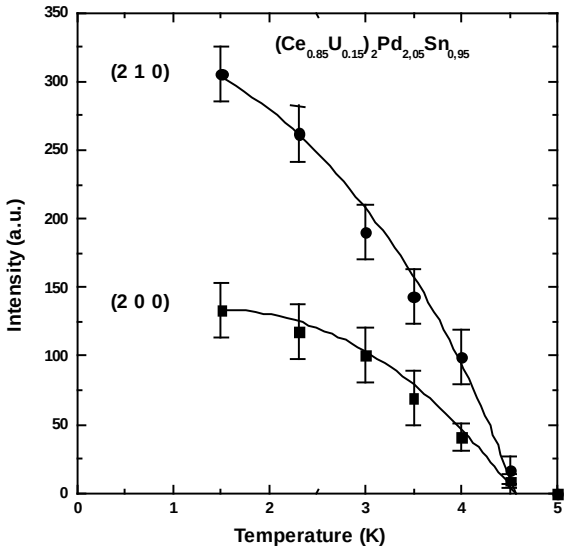

Figure 7. Temperature dependence of the intensity of magnetic reflections (2 0 0) and (2 1 0) observed for $(Ce_{0.85}U_{0.15})_2Pd_{2.05}Sn_{0.95}$ stannide.

Table 3. Definition of the six ground states and corresponding degenerate structures for the two propagation vectors $\boldsymbol{k} = (0\,0\,0)$ and $\boldsymbol{k} = (0\,0\,1/2)$ ($P4/mbm$ space group; (4h) Wyckoff crystallographic site).

Wave vector	Ground state	Equivalent configurations
$\boldsymbol{k} = (0\,0\,0)$	NC1	NC2, NC3, NC4, C1
	FC	C3 ($\phi = 0$)
	C2	C3 ($\phi = \pi$)
$\boldsymbol{k} = (0\,0\,1/2)$	Γ_9	Γ_1, Γ_3, Γ_5, Γ_7
	Γ_2	Γ_{10} ($\phi = 0$)
	Γ_8	Γ_{10} ($\phi = \pi$)

The sum in (3) is now calculated considering pair interactions with neighbouring atoms at distances $\leqslant 2a$, a being the crystallographic unit-cell parameter in the ab-plane. This corresponds to about $N = 300$ atoms and to 5% convergence of the sum.

The relative stability of the antiferromagnetic U_2Pd_2Sn and ferromagnetic $Ce_2Pd_{2.05}Sn_{0.95}$ structures is obtained considering all irreducible magnetic configurations resulting from magnetic group theory applied to $P4/mbm$ space group: (4h) Wyckoff position (the crystallographic site for (Ce, U) atoms) and the two propagation vectors $\boldsymbol{k} = (0\,0\,0)$ and $\boldsymbol{k} = (0\,0\,1/2)$ [7, 8, 23]. More precisely, there are eight configurations (basis vectors for irreducible representations) in the case of $\boldsymbol{k} = (0\,0\,0)$: these are labelled [7] FC, C1, C2, NC1, NC2, NC3, NC4, C3, where F stands for ferromagnetic, C for collinear and NC for non-collinear (figure 8); eight configurations are also obtained in the case of $\boldsymbol{k} = (0\,0\,1/2)$ [23]: they are now labelled Γ_2, Γ_9, Γ_8, Γ_5, Γ_3, Γ_1, Γ_7, Γ_{10} (figure 8). We have shown [17] that the Heisenberg Hamiltonian in (2) leads to an energy degeneracy of several structures, so that only six ground states (table 3) have to be considered in our calculation.

U_2Pd_2Sn [8] and $Ce_2Pd_{2.05}Sn_{0.95}$ [11] are respectively ordered according to the $\boldsymbol{k} = (0\,0\,0)$ non-collinear NC1 and FC magnetic arrangements. Figure 9 gives the map of the NC1 and FC stability domains for different values of the Fermi wavevector components k_F and k_{Fz}.

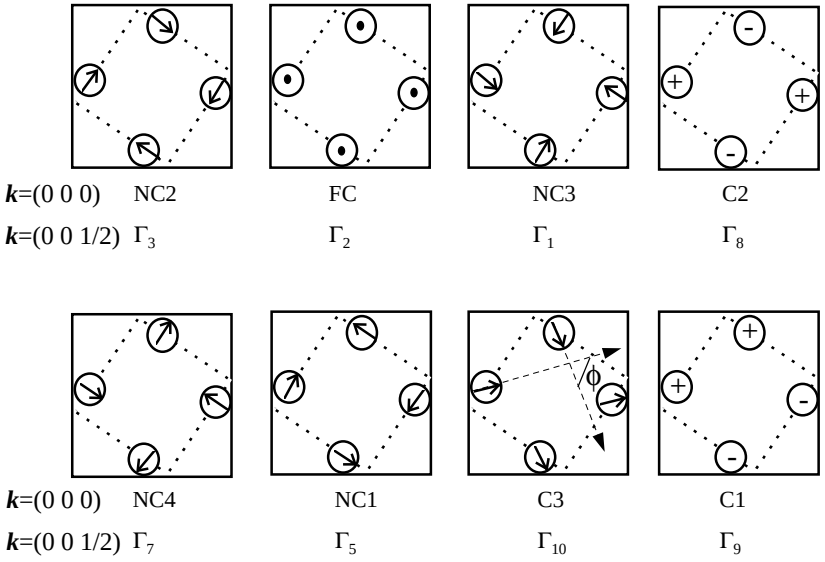

Figure 8. Magnetic structures (basis vectors for irreducible representations [7, 23]) for $P4/mbm$ space group, (4h) Wyckoff position and the two propagation vectors $\boldsymbol{k} = (0\,0\,0)$ and $\boldsymbol{k} = (0\,0\,1/2)$. The magnetic (Ce, U) atoms only are represented in the figure. The (Ce–U) magnetic moments into adjacent planes along c-axis are reversed for the structures relative to $\boldsymbol{k} = (0\,0\,1/2)$.

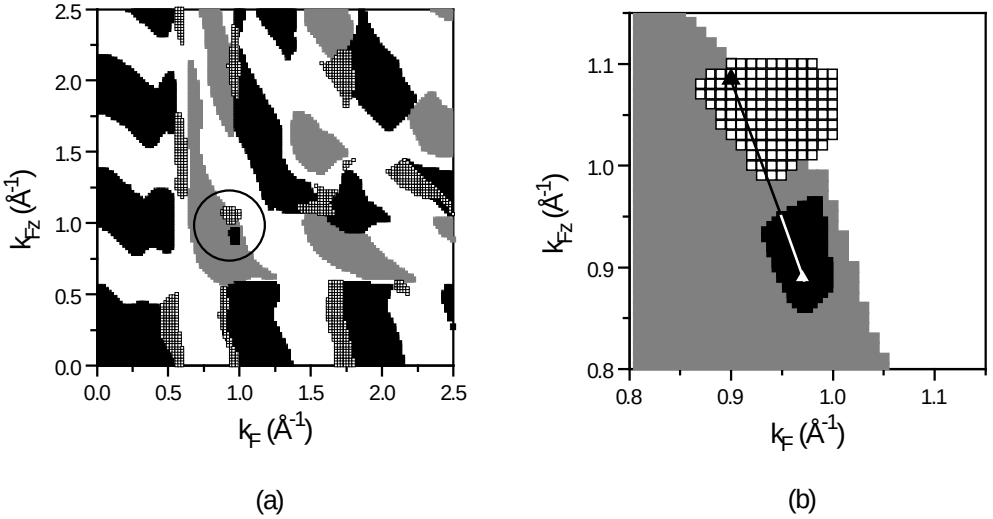

Figure 9. Stability domains versus Fermi wave vector of the NC1, FC and $\Gamma_{10}(\phi = \pi)$ magnetic structures: (a) for $0 \leqslant k_F, k_{Fz} \leqslant 2.5$ and (b) for $0.8 \leqslant k_F, k_{Fz} \leqslant 1.15$ leading to an efficient representation of the $U_2(Ni_{1-x}Pd_x)_2Sn$ magnetic phase diagram. (Squared regions: NC1 structure using $a = 0.7592$ nm and $c = 0.3770$ nm [8]. Black regions: FC structure using $a = 0.7708$ nm and $c = 0.3957$ nm [9]. Grey regions: $\Gamma_{10}(\phi = \pi)$ structure using $a = 0.7214$ nm and $c = 0.3707$ nm [23].)

The NC1 and FC stability domains are respectively calculated from equation (2) using the R'_{ij} distances deduced from experimental R_{ij} interactomic distances of U_2Pd_2Sn (neutron powder diffraction data, $T = 1.5$ K [8]) and $Ce_2Pd_{2.05}Sn_{0.95}$ (neutron powder diffraction data, $T = 10$ K [9]). In order to facilitate the following discussion, the stability domain of

the collinear $\Gamma_{10}(\phi = \pi)$ magnetic structure adopted by U_2Ni_2Sn [23] is also presented in figure 9. Here again, we used the R_{ij} interatomic distances determined at 36 K by neutron powder diffraction. The fact of using different atomic position parameters for the calculation of the stability of each magnetic structure explains the existence of some overlaps. For readability, the stability of the three other ground states, C2, Γ_9 and Γ_2 (table 3), are not shown in figure 9 (this explains the white region in the map).

Previously, we have studied the magnetic transition $\Gamma_{10}(\phi = \pi) \rightarrow$ NC1 in the $U_2(Ni_{1-x}Pd_x)_2Sn$ system [17]. The anisotropic RKKY model was efficient to describe the proximity of these two magnetic structures on the ground-state map (figure 9). We focused on the lowest (k_F, k_{Fz})-range underlined in figure 9(a) which allows us to reproduce correctly the $T_N = f(x)$ curve of the antiferromagnetic $U_2(Ni_{1-x}Pd_x)_2Sn$ system [17]. Naturally, we did not exclude other closed $\Gamma_{10}(\phi = \pi)$ and NC1 stability domains occurring on the map since we cannot yield to the number of conduction electrons per unit cell. In the present analysis performed on the $(Ce_{1-x}U_x)_2Pd_{2.05}Sn_{0.95}$ system, we see that the anisotropic RKKY model tends, in the $0 \leqslant k_F, k_{Fz} \leqslant 2.5$ range, to largely stabilize the FC magnetic structure (figure 9) near the NC1 domain in agreement with the experimental data. From that neighbouring FC and NC1 domains, we now calculate the magnetic phase diagram of the $(Ce_{1-x}U_x)_2Pd_{2.05}Sn_{0.95}$ system. As a first step, we select two (k_F, k_{Fz})-points, relative to U_2Pd_2Sn and $Ce_2Pd_{2.05}Sn_{0.95}$ compounds, on their respective NC1 and FC stability domains. The U_2Pd_2Sn compound is then represented by the black triangle (figure 9(b)), located near the point previously selected for $x = 1$ in $U_2(Ni_{1-x}Pd_x)_2Sn$ system [17]; and $Ce_2Pd_{2.05}Sn_{0.95}$ by the white triangle (figure 9(b)), selected in order to fit the order–disorder temperature ratio of these two compounds (T_N for U_2Pd_2Sn, T_C for $Ce_2Pd_{2.05}Sn_{0.95}$).

Then, from these two points, we deduced the $((T_C, T_N)$–$x)$ magnetic phase diagram for $(Ce_{1-x}U_x)_2Pd_{2.05}Sn_{0.95}$, on the basis of the following assumptions :

- a constant value of j_{sf} interaction with x;
- linear dependence with x of the Fermi wavevector $\boldsymbol{k}_F$ between the two selected points;
- linear dependence with x of the crystallographic parameters (a, c) and Ce–U atomic position parameter, between those measured at $T = 10$ K for $Ce_2Pd_{2.05}Sn_{0.95}$ [5] and $T = 1.5$ K for U_2Pd_2Sn [8];
- linear dependence on x of the de Gennes factor G for (Ce, U) atoms (Ce^{3+} ($G = 0.179$) and U^{3+} ($G = 1.841$) at the ends).

The 'theoretical' diagram we obtained is shown in figure 10, together with the experimental data. In the light of the complexity of the $(Ce_{1-x}U_x)_2Pd_{2.05}Sn_{0.95}$ system, the agreement with experimental magnetic ordering temperature of the reduced calculated temperatures ((T_C, T_N) against x) as well as the crossover composition x from FC ferromagnetic to NC1 antiferromagnetic ground state is good. Indeed, a slight deviation from the idealized linear evolution with x of the physical parameters j_{sf}, G, k_F will affect the magnetic phase diagram. For instance the hybridization of the 5f (U) and 4f (Ce) electrons with the d (Pd) or p (Sn) bands of the ligands which would tend to lower the G factor is not quantified. Moreover, even if we quantified long range magnetic interaction leading to an accurate description of the interaction of a spin with its magnetic surroundings, we do not quantify with the mean-field theory the magnetic structure entropy of configuration. This entropy term cannot be neglected when magnetic frustrations are involved as it could be expected around the crossover from FC ferromagnetic to NC1 antiferromagnetic structure. This could also explain the discrepancy at the critical composition between the experimental and calculated phase diagram. This configurational entropy could be quantified using the Monte Carlo method. If the $\Gamma_{10}(\phi = \pi)$ ground state is present together with FC and NC1 structures between the two

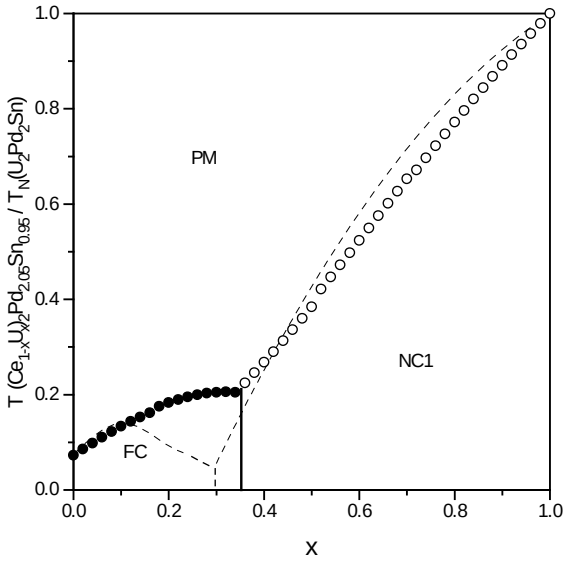

Figure 10. $((T_C,\ T_N)$–$x)$ calculated phase diagram of the $(Ce_{1-x}U_x)_2Pd_{2.05}Sn_{0.95}$ system: ● calculated T_C; ○ calculated T_N; – – – experimental values (T_C or T_N).

selected points (grey region in figure 9), we do not find it for the calculated $((T_C,\ T_N)$ against $x)$ diagram. This is due to the variation of the unit-cell parameters with x, which contributes to destabilize the $\Gamma_{10}(\phi = \pi)$ ground state.

4. Conclusion

X-ray diffraction studies on the $(Ce_{1-x}U_x)_2Pd_{2.05}Sn_{0.95}$ system reveal a single phase crystal structure (tetragonal U_2Fe_2Sn type) from $x = 0$ to $x = 1$. The unit-cell parameters are decreasing with increasing U content in agreement with the size of (Ce, U) metallic radius. The magnetic transition sequence 'paramagnetic $\rightarrow$ antiferromagnetic $\rightarrow$ ferromagnetic' present in the $Ce_2Pd_{2.05}Sn_{0.95}$ compound is no longer evidenced in the $(Ce_{1-x}U_x)_2Pd_{2.05}Sn_{0.95}$ system for $x \geqslant 0.1$. The substitution of U atoms for Ce stabilizes the ferromagnetic phase to the detriment of the antiferromagnetic one, so that the paramagnetic $\rightarrow$ ferromagnetic transition is the only magnetic transition to be observed for $x < 0.30$. The stability of the ferromagnetic phase (up to $x \simeq 0.30$) is confirmed by neutron powder diffraction on $(Ce_{0.85}U_{0.15})_2Pd_{2.05}Sn_{0.95}$. In the $0 \leqslant x < 0.30$ composition range, T_C goes through a maximum at $x \simeq 0.1$–0.15. The composition $x \simeq 0.3$ corresponds to a change in the low temperature magnetic properties of $(Ce_{1-x}U_x)_2Pd_{2.05}Sn_{0.95}$ compounds, from ferromagnetic to antiferromagnetic behaviour. For x growing from 0.30 to 1, a continuous increase of the antiferromagnetic transition temperature T_N is then observed. A modelling of the $((T_C,\ T_N)$–$x)$ magnetic phase diagram is obtained in the framework of anisotropic (non-spherical Fermi surface for the conduction electrons) RKKY magnetic interactions. The calculated x value of the ferromagnetic $\rightarrow$ antiferromagnetic crossover is close to that experimentally obtained. The present study, together with the previous one dedicated to the $U_2(Ni_{1-x}Pd_x)_2Sn$ system, highlights the fact that the magnetic interactions between localized magnetic moments in this family of stannides are consistently modelled within anisotropic RKKY coupling (ellipsoidal, instead of spherical Fermi surface).

References

[1] Mirambet F, Chevalier B, Fournès L, Gravereau P and Etourneau J 1994 *J. Alloys Compounds* **203** 29
[2] Sanchez J P, Colineau E, Jeandey C, Oddou J L, Rebizant J, Seret A and Spirlet J C 1995 *Physica* B **206/207** 531
[3] Mirambet F, Fournès L, Chevalier B, Gravereau P and Etourneau J 1994 *J. Magn. Magn. Mater.* **138** 244
[4] Gordon R A and DiSalvo F J 1996 *J. Alloys Compounds* **238** 57
[5] Fourgeot F, Gravereau P, Chevalier B, Fournès L and Etourneau J 1996 *J. Alloys Compounds* **238** 102
[6] Gordon R A, Ijiri Y, Spencer C M and DiSalvo F J 1995 *J. Alloys Compounds* **224** 101
[7] Purwanto A, Robinson R A, Havela L, Sechovsky V, Svoboda P, Nakotte H, Prokes K, de Boer F R, Seret A, Winand J M, Rebizant J and Spirlet J C 1994 *Phys. Rev.* B **50** 6792
[8] Laffargue D, Bourée F, Chevalier B, Roisnel T, Gravereau P and Etourneau J 1997 *J. Magn. Magn. Mater.* **170** 155
[9] Laffargue D, Fourgeot F, Bourée F, Chevalier B, Roisnel T and Etourneau J 1996 *Solid State Commun.* **100** 575
[10] Pinto R P, Amado M M, Braga M E, de Azevedo M M P, Sousa J B, Chevalier B and Etourneau J 1997 *J. Appl. Phys.* **81** 4182
[11] Laffargue D, Roisnel T, Chevalier B and Bourée F 1997 *J. Alloys Compounds* **262/263** 219
[12] Chevalier B, Fourgeot F, Laffargue D, Pöttgen R and Etourneau J 1998 *J. Alloys Compounds* **275–277** 537
[13] Fourgeot F, Chevalier B, Laffargue D and Etourneau J 1998 *J. Magn. Magn. Mater.* **182** 124
[14] Tran V H, Zolnierek Z, Zaleski A J and Noel H 1997 *Solid State Commun.* **101** 709
[15] Hauser R, Michor H, Bauer E, Hilscher G and Kaczorowski D 1997 *Physica* B **230–232** 211
[16] Kaczorowski D, Rogl P and Hiebl K 1996 *Phys. Rev.* B **54** 9891
[17] Bordère S, Buzdin S, Chevalier B, Laffargue D and Etourneau J 1997 *J. Magn. Magn. Mater.* **175** 263
[18] Rodriguez-Carvajal J 1993 *Physica* B **192** 55
[19] Freeman A J and Desclaux J P 1979 *J. Magn. Magn. Mater.* **12** 11
[20] Sears V F 1992 *Neutron News* **3** 26
[21] Brown P J 1970 *International Tables for Crystallography* vol C(4.4.4), ed A J C Wilson (Dordrecht: Kluwer)
[22] Laffargue D 1997 *Thesis* University of Bordeaux I No 1734
[23] Bourée F, Chevalier B, Fournès L, Mirambet F, Roisnel T, Tran V H and Zolnierek Z 1994 *J. Magn. Magn. Mater.* **138** 307
[24] Laffargue D, Bourée F, Chevalier B, Roisnel T and Bordère S 1998 *J. Alloys Compounds* **271–273** 444
[25] Bourée F private communication
[26] Ruderman M A and Kittel C 1954 *Phys. Rev.* **96** 99
[27] Kasuya T 1956 *Prog. Theor. Phys.* **16** 45
[28] Yosida K 1957 *Phys. Rev.* **106** 893
[29] de Gennes P G 1962 *J. Physique Radium* **23** 510